

# Neutrino propagation hinders fast pairwise flavor conversions

**Shashank Shalgar, Ian Padilla-Gay, and Irene Tamborra**

Niels Bohr International Academy and DARK, Niels Bohr Institute, University of Copenhagen, Blegdamsvej 17, 2100, Copenhagen, Denmark

E-mail: [shashank.shalgar@nbi.ku.dk](mailto:shashank.shalgar@nbi.ku.dk), [ian.padilla@nbi.ku.dk](mailto:ian.padilla@nbi.ku.dk), [tamborra@nbi.ku.dk](mailto:tamborra@nbi.ku.dk)

**Abstract.** Neutrino flavor conversions may dramatically affect the inner working of compact astrophysical objects as well as the synthesis of new elements. We present the first sophisticated numerical solution of the neutrino flavor conversion within a (2+1+1) dimensional setup: we include the advective term in the neutrino equations of motion and track the flavor evolution in two spatial dimensions, one angular variable, and time. Notably, the advective term hinders the development of neutrino pairwise conversions, if the conditions favoring such conversions (i.e., crossings between the angular distributions of  $\nu_e$  and  $\bar{\nu}_e$  or a non-negligible flux of neutrinos traveling backward with respect to the main propagation direction) exist for time scales shorter than the typical time scale of the advective term. As a consequence, fast pairwise conversions can only occur when the conditions favoring flavor conversions are self-sustained and global, such as the ones induced by the lepton emission self-sustained asymmetry (LESA) in core-collapse supernovae. Our work highlights the major impact of the dynamical evolution of the neutrino field on the growth of flavor instabilities and the strong interplay between classical and quantum effects. Critical limitations of the linear stability analysis, used to predict neutrino flavor instabilities, are also pointed out.

---

## Contents

<b>1</b>	<b>Introduction</b>	<b>1</b>
<b>2</b>	<b>Fast pairwise neutrino flavor conversion</b>	<b>3</b>
2.1	Equations of motion	3
2.2	Instability parameter	4
<b>3</b>	<b>Neutrino flavor evolution in a two-dimensional box</b>	<b>4</b>
3.1	Model setup	5
3.2	Numerical implementation	6
3.3	Growth of the flavor instability	8
<b>4</b>	<b>Role of the advective term in the neutrino evolution equation</b>	<b>9</b>
4.1	Impact of the advective term on the neutrino distributions	9
4.2	Flavor evolution in the one stripe configuration	11
4.3	Flavor evolution in the two stripe configuration	12
4.4	Flavor evolution in the one dot configuration	14
<b>5</b>	<b>Outlook and conclusions</b>	<b>14</b>

---

## 1 Introduction

In the interior of neutrino dense astrophysical environments, such as neutron star mergers and core-collapse supernovae (SNe), neutrinos experience a non-negligible potential due to the presence of other neutrinos. This potential is analogous to the one due to electrons in the well known Mikheev-Smirnov-Wolfenstein (MSW) effect [1, 2]. The neutrino-neutrino scattering gives rise to an extremely fascinating phenomenology, inducing non-linear effects in the neutrino equations of motion [3, 4]. Notably, as a result of the non-linear nature of the evolution equations, the flavor evolution of neutrinos with different momenta is correlated.

The non-linearity of the neutrino equations of motion in compact astrophysical objects makes the solution of the neutrino flavor evolution extremely challenging, even when unrealistic simplifying assumptions are made. One of the first successful self-consistent calculations of neutrino flavor evolution including neutrino-neutrino interactions has been performed assuming spherical symmetry and instantaneous decoupling of all neutrino flavors at the same radius [5–9], the so-called “neutrino-bulb model.” Despite being extremely simplified, the calculation of neutrino flavor evolution within the bulb model still proves to be challenging. In fact, it requires the numerical solution of several millions of differential equations that may take up to several hundred CPU-hours depending on the desired accuracy.

Any relaxation of the assumptions of the neutrino-bulb model makes the numerical solution of the flavor problem unfeasible. However, semi-analytical techniques proved that the non-linear nature of the problem implies that the bulb model provides different results than the ones obtained when some of the assumptions of this model are relaxed [10–13].

In addition, since the decoupling of different flavors occurs at different radii and neutrinos undergo flavor-dependent interactions, the initial angular distributions are flavor dependent. In some circumstances, this can lead to coherent pairwise conversion of neutrinos [14–16]. Pairwise conversions are fast in the sense that their characteristic time scale

is proportional to the neutrino number density, instead than the typical neutrino vacuum frequency [16]. Favorable conditions for fast flavor conversions may occur in the proximity of the neutrino decoupling region [15–18]. Therefore, fast pairwise conversions may have important implications for the neutrino-driven explosion mechanism in SNe as well as the nucleosynthesis of heavy elements.

One of the conditions that has been identified as being relevant to the development of fast pairwise conversions is the existence of crossings in the electron neutrino lepton number (ELN) or a non-negligible flux of neutrinos propagating in the backward direction [16, 19, 20]. In a spherically symmetric SN, the occurrence of ELN crossings in the proximity of the decoupling region requires a sharp radial evolution of the baryon density, with electron neutrino and antineutrino number densities being comparable [21, 22]. Moreover, localized regions of ELN crossings may also occur in the early SN stages. It is not clear whether in this case the neutrino flavor evolution may affect the SN physics on a macroscopic scale, or whether there are fast neutrino conversions at all [21]. In neutron star mergers, the occurrence of ELN crossings seems to be favored by the more complex geometry and the natural excess of  $\bar{\nu}_e$ 's over  $\nu_e$ 's [23, 24].

The major implications of the eventual occurrence of fast pairwise conversions in compact astrophysical objects has triggered a remarkable effort from the community to better grasp this phenomenon [21, 22, 25–31], but there is a long road ahead. In fact, one of the major complications is related to the numerical solution of this problem with high enough spatial and angular resolution, as dictated by the high frequency imposed by the neutrino fast conversions.

Given the complications induced by the non-linear nature of the system, and due to the spontaneous breaking of spatial and axial symmetries [11, 12], a minimum of two spatial dimensions is required to properly grasp the physics of the system. We here present the first sophisticated (2+1+1) dimensional modeling of the fast pairwise conversions in compact astrophysical objects; we solve the equations of motion in two spatial dimensions, one angular variable, and time and we include the advective term in the equations of motion. Within a simplified framework mimicking patches of the dense SN core, we explore the time evolution of the neutrino and antineutrino distributions in the presence of localized ELN crossings and of extended regions of ELN crossings similar to the ones induced by the lepton emission self-sustained asymmetry (LESA) [32].

The main goal of our work is to investigate under which conditions flavor instabilities may grow within a dynamical system. To do that, we explore three different scenarios reproducing global and localized regions of ELN crossings similar to the ones found in hydrodynamical simulations of SNe [22, 27, 29, 30, 32]. We also introduce the “instability parameter” and generalize the criteria under which fast pairwise conversions may occur.

This paper is organized as follows. In Sec. 2 we discuss the conditions favoring the occurrence of fast pairwise conversions proposed in the literature and adapt them to our (2+1+1) dimensional model. We also provide a generalization of the criteria leading to favorable conditions for fast conversions by introducing the “instability parameter.” In Sec. 3, we describe the setup of our (2+1+1) model and its numerical implementation. In Sec. 4, for the first time, we explore the impact of the advective term on the ELN evolution and on the growth of flavor instabilities. We then explore the flavor evolution when an extended stripe of ELN crossings exists, when two ELN stripes are considered and they move towards each other, and when only one localized ELN excess occurs. Finally, an outlook of our work and conclusions are presented in Sec. 5.

## 2 Fast pairwise neutrino flavor conversion

The non-linearity induced by the neutrino-neutrino interactions makes the flavor evolution strongly dependent on the geometry and the number of dimensions of the system. Since at least two spatial dimensions are required for exploring any eventual effect of the advective term on the neutrino angular distributions, we explore the evolution of the (anti)neutrino angular distributions in time, within a two-dimensional (2D) box, and for one angular variable. In this Section, we introduce the neutrino equations of motion in the 2D box and generalize the criteria leading to fast pairwise conversions by introducing the “instability parameter.”

### 2.1 Equations of motion

Our system consists of a 2D box with width and height given by  $L_x$  and  $L_y$  and periodic boundary conditions. For each point  $(x, y)$  in the box,  $2 \times 2$  density matrices describe the neutrino and antineutrino fields, respectively, at time  $t$ :

$$\rho(\vec{x}, \theta, t) = \begin{pmatrix} \rho_{ee} & \rho_{ex} \\ \rho_{ex}^* & \rho_{xx} \end{pmatrix} \quad \text{and} \quad \bar{\rho}(\vec{x}, \theta, t) = \begin{pmatrix} \bar{\rho}_{ee} & \bar{\rho}_{ex} \\ \bar{\rho}_{ex}^* & \bar{\rho}_{xx} \end{pmatrix}. \quad (2.1)$$

The density matrix of neutrinos is normalized such that  $\text{tr}(\rho) = 1$  and we fix the asymmetry between neutrinos and antineutrinos such that  $\text{tr}(\bar{\rho}) = a$ . For each point  $(x, y)$  in the box, the (anti)neutrino field has a distribution in momentum. For the sake of simplicity and since we intend to focus on fast pairwise conversions, we assume all (anti)neutrinos have the same energy, and the momentum is only determined by the angle  $\theta$  with respect to the  $y$ -axis.

The flavor evolution is determined by the following equations of motion for neutrinos and antineutrinos:

$$i \left( \frac{\partial}{\partial t} + \vec{v} \cdot \vec{\nabla} \right) \rho(\vec{x}, \theta, t) = [H(\theta), \rho(\vec{x}, \theta, t)], \quad (2.2)$$

$$i \left( \frac{\partial}{\partial t} + \vec{v} \cdot \vec{\nabla} \right) \bar{\rho}(\vec{x}, \theta, t) = [H(\theta), \bar{\rho}(\vec{x}, \theta, t)]. \quad (2.3)$$

The advective term,  $\vec{v} \cdot \vec{\nabla}$ , depends on the velocity of the (anti-)neutrino field  $\vec{v}$ . The latter has modulus equal to the speed of light and direction along the direction of propagation. The Hamiltonian,  $H$ , consists of a vacuum term that depends on the neutrino mixing parameters, a term describing the interactions of neutrinos with the matter background, and a self-interaction term, see e.g. [3].

Since we intend to focus on fast pairwise conversions, we neglect the vacuum term in the Hamiltonian. We also ignore the matter term as it is not relevant to our purposes. In addition, as we will discuss in Sec. 4, we neglect the collision term. The Hamiltonian is then

$$H(\theta) = \mu \int d\theta' [\rho(\vec{x}, \theta', t) - \bar{\rho}(\vec{x}, \theta', t)] [1 - \cos(\theta - \theta')], \quad (2.4)$$

where  $\mu$  represents the strength of the neutrino-neutrino interaction

$$\mu = 10^5 \text{ km}^{-1}. \quad (2.5)$$

Significant evolution in the number of (anti-)neutrinos can occur only if the off-diagonal term of the Hamiltonian is not very small compared to the diagonal term. In the case of

neutrino-neutrino interactions, the magnitude of the off-diagonal component of the Hamiltonian is a dynamical quantity that is determined by the momentum distribution of the density matrices. For a given initial angular and spatial distribution, whether there will be significant flavor evolution depends on the temporal evolution of the off-diagonal elements of the density matrices which are connected to the probability of flavor transition. If the off-diagonal components of the density matrices grow with time (i.e., a flavor instability occurs), they will eventually lead to a change in the diagonal components of the density matrices which are directly connected to the spatial and temporal evolution of the number density of the different flavors.

For the sake of simplicity and without loss of generality, in what follows, we assume  $\rho_{xx}(t = 0 \text{ s}) = \bar{\rho}_{xx}(t = 0 \text{ s}) = 0$ ,  $a = 0.5$ , and  $L_x = L_y = 100 \text{ km}$ . If all off-diagonal terms of the density matrices are zero at  $t = 0 \text{ s}$ , then they will remain zero in the absence of the linear terms of the Hamiltonian (vacuum or matter term). In order to reproduce situations where non-zero off-diagonal terms may be induced by stochastic hydrodynamical fluctuations or induced by the linear terms of the Hamiltonian, we seed  $\rho_{ex}(t = 0 \text{ s}), \bar{\rho}_{ex}(t = 0 \text{ s}) \neq 0$  as detailed later. We also assume a constant  $\mu$  across the whole 2D box and impose periodic boundary conditions. As we will see in Sec. 4, this allows to track the flavor evolution within our (2+1+1) setup with a reasonable number of CPU-hours.

## 2.2 Instability parameter

The rate of growth of the off-diagonal terms of the density matrices (and therefore of the flavor instability) can be estimated by using the linear stability analysis for given initial conditions [10, 16]. In particular, Ref. [16] found that fast pairwise conversions may be induced by ELN crossings or in the presence of a non-negligible backward flux. In the case of ELN crossings, the growth of flavor instabilities may be affected by the depth of ELN crossings [20, 33].

We here introduce the “instability parameter” that depends on the shape of the angular distributions of  $\nu_e$  and  $\bar{\nu}_e$  and it is approximately proportional to the growth rate of the off-diagonal components of the density matrices:

$$\zeta = \frac{I_1 I_2}{(I_1 + I_2)^2} \quad (2.6)$$

with

$$I_1 = \int_0^{2\pi} [\rho_{ee}(\theta) - \bar{\rho}_{ee}(\theta)] d\theta \quad \text{for} \quad \rho_{ee}(\theta) > \bar{\rho}_{ee}(\theta) \quad (2.7)$$

$$I_2 = \int_0^{2\pi} [\bar{\rho}_{ee}(\theta) - \rho_{ee}(\theta)] d\theta \quad \text{for} \quad \bar{\rho}_{ee}(\theta) > \rho_{ee}(\theta) . \quad (2.8)$$

It should be noted that, since the definition of  $\zeta$  contains two powers of  $I_{1,2}$  in the numerator and in the denominator,  $\zeta$  is independent of the overall normalization of the density matrices. The  $\zeta$  parameter is zero when there is no ELN crossing or when there is no backward flux, therefore it generalizes the criteria outlined in Ref. [16].

## 3 Neutrino flavor evolution in a two-dimensional box

We explore three configurations of our 2D box. The first scenario corresponds to the case where neutrinos and antineutrinos are initially located along a stripe in the  $(x, y)$  plane. This

would mimic the evolution of flavor conversions in the case of an extended region of ELN crossings such as in the presence of LESA. The second scenario is similar to the previous one, but we assume two stripes moving towards each other, such as expected in the decoupling region. The third scenario corresponds to the case where neutrinos and antineutrinos are initially localized in a small region in the  $(x, y)$  plane which should mimic the evolution of random fluctuations occurring within the inner SN core. In the following, we will introduce the numerical framework adopted to explore the flavor evolution in all these configurations.

### 3.1 Model setup

We define a 2D spatial grid with length  $L_x = L_y = 100$  km which is identical in all simulations. The “one stripe configuration” is shown in the top left panel of Fig. 1. It corresponds to the initial box configuration consisting of neutrinos localized along a stripe, which is homogeneous along the  $y$ -axis and distributed according to a Gaussian along the  $x$ -axis as displayed in the 1D projection in the middle panel of Fig. 1. The non-zero diagonal terms of the density matrix are defined as follows

$$\rho_{ee}, \bar{\rho}_{ee} \propto \exp \left[ -\frac{(x - x_0)^2}{2\sigma^2} \right], \quad (3.1)$$

with  $\sigma = 8\%L_x$  and the center of the distribution  $x_0 = 1/5L_x$ .

At  $t = 0$  s, for each  $(x, y)$  the angular distributions of neutrinos and antineutrinos are fixed to be two top hat angular distributions,

$$\rho_{ee}(\theta) = \begin{cases} g & |\theta| < b \\ 0 & |\theta| \geq b \end{cases}, \quad (3.2)$$

$$\bar{\rho}_{ee}(\theta) = \begin{cases} \bar{g} & |\theta| < \bar{b} \\ 0 & |\theta| \geq \bar{b} \end{cases}, \quad (3.3)$$

with  $b$  being the opening angle of the  $\nu_e$  angular distribution (assumed to be  $\pi/6$  unless otherwise specified) and  $\bar{b} = \pi$  being the one of  $\bar{\nu}_e$ . This configuration would mimic what should happen in the presence of LESA, when the ELN changes its sign. A sketch of the initial  $\nu_e$  and  $\bar{\nu}_e$  angular distributions for three selected points across the stripe is shown in the bottom panel of Fig. 1.

Note that we assume that the angular distribution of  $\nu_e$  is forward peaked and the  $\bar{\nu}_e$  one is isotropic. However, in a realistic framework, the angular distributions of neutrinos and antineutrinos are both forward peaked after decoupling. As we will see later, we focus on a more extreme scenario since any growth of a flavor instability would be further suppressed, if both distributions are assumed to be forward peaked at  $t = 0$  s. Moreover, the occurrence of fast neutrino oscillations requires that the values of the heights  $(g, \bar{g})$  and the widths  $(b, \bar{b})$  of the angular distributions are different for neutrinos and antineutrinos.

The “two stripe configuration” is shown in the middle top panel of Fig. 1 and would mimic the case of two (anti)neutrino fronts crossing each other. The (anti)neutrino field is now distributed along two Gaussian distributions as in Eq. 3.1, one on the left and one on the right of the 2D box with mean values  $x_{0,L} = 3/10 \times L_x$  and  $x_{0,R} = 7/10 \times L_x$ ;  $\sigma$  is the same as in the single stripe scenario.

The “one dot configuration” is shown in the right top panel of Fig. 1. It has been obtained by assuming

$$\rho_{ee}, \bar{\rho}_{ee} \propto \exp \left[ -\frac{(x - x_0)^2}{2\sigma^2} \right] \exp \left[ -\frac{(y - y_0)^2}{2\sigma^2} \right], \quad (3.4)$$

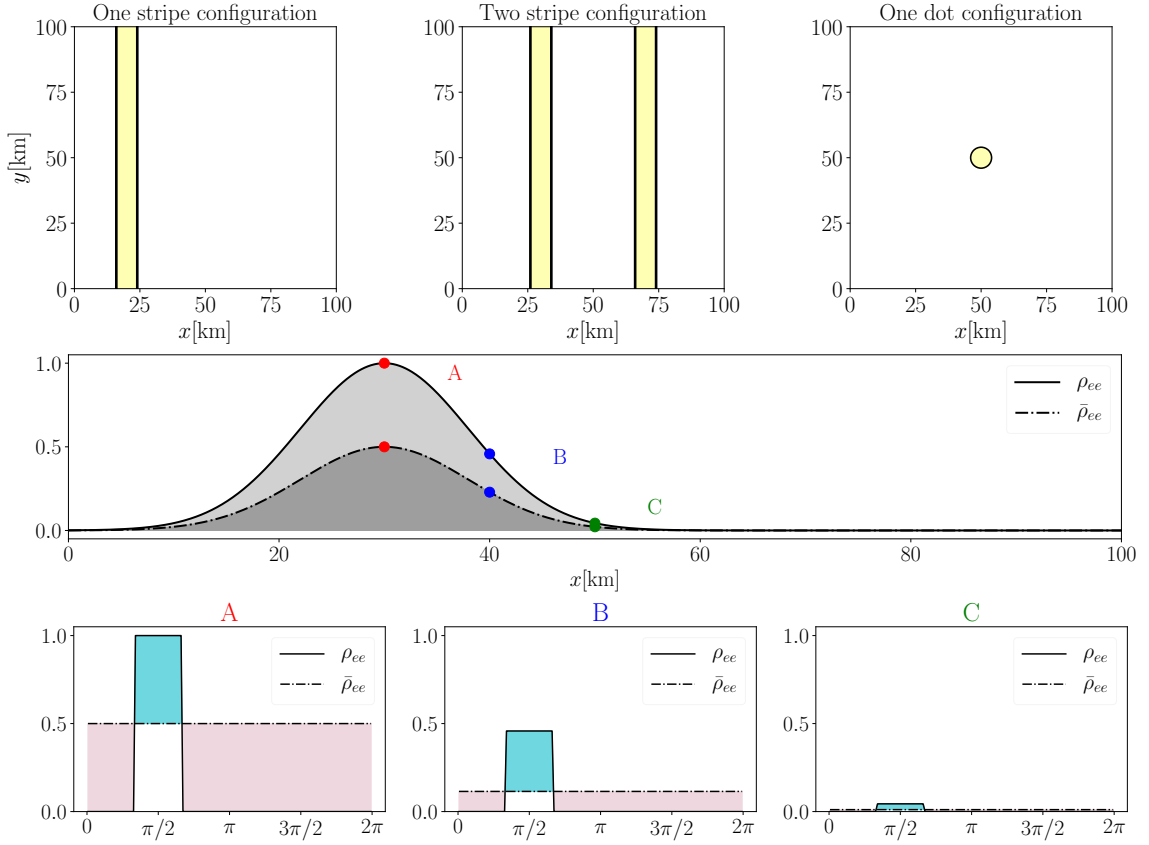


**Figure 1.** *Top:* Sketch of the 2D box at  $t = 0$  s for the three configurations adopted in this paper: “one stripe configuration” (on the left), “two stripe configuration” (in the middle), and “one dot configuration” (on the right), see main text for more details. *Middle:* 1D projection of the stripe or dot configuration to show  $\rho_{ee}$  (continuous line) and  $\bar{\rho}_{ee}$  (dot-dashed line) as a function of  $x$ . *Bottom:*  $\nu_e$  and  $\bar{\nu}_e$  angular distributions for the three points A, B, and C highlighted in the middle panel, respectively from left to right.

with  $x_0 = y_0 = 1/2L_x$ . This scenario would mimic the evolution of ELN crossings generated by stochastic fluctuations in the proximity of the decoupling region.

### 3.2 Numerical implementation

We perform numerical simulations with different initial conditions, while keeping the overall architecture of the numerical simulations and the grid size unchanged. For each  $(x, y)$  point, we define the angular distributions of neutrinos and antineutrinos as described in Sec. 3.1 and evolve the (anti)neutrino equation of motions according to Eqs. 2.2, 2.3. In the numerical runs, we adopt the following number of spatial and angular bins:  $N_x = N_y = 300$  and  $N_\theta = 150$ . We use an adaptive method for the temporal evolution of the system. Note, however, that for the cases without the advective term, the number of spatial bins is not relevant since the spatial gradient in the advective term is zero. Although, we impose periodic boundary conditions on our box, we let the stripe configurations evolve within a time interval such that (anti)neutrinos never cross the boundaries.

The spatial gradient on the left-hand-side of Eqs. 2.2 and 2.3 can lead to numerical instabilities, if a sufficient number of spatial bins is not used. This problem can be made less

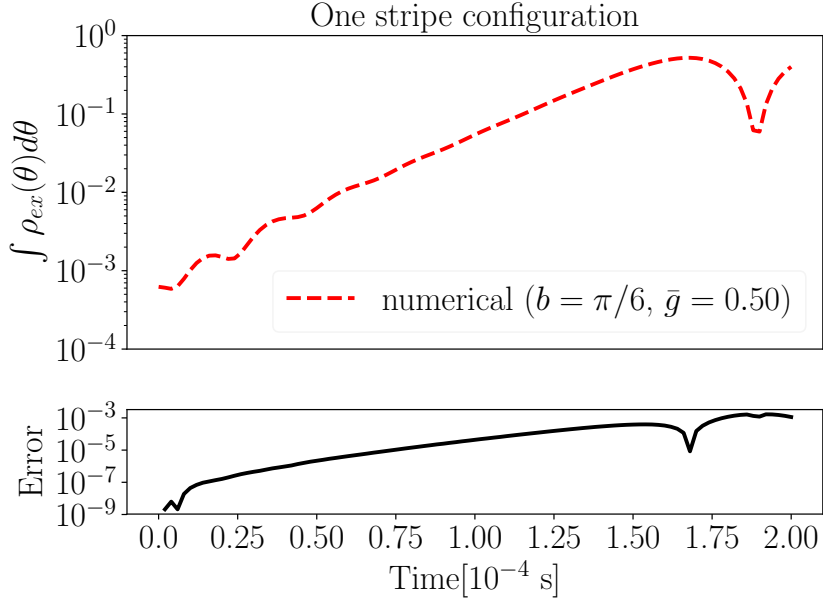


**Figure 2.** *Top:* Growth rate of  $\int d\theta \rho_{ex}(\theta)$  as a function of time for a comoving point with maximum  $\rho_{\text{tot}} = \rho_{ee} + \bar{\rho}_{ee} + 2\rho_{xx} = \text{const.}$  in the “one stripe configuration” without the advective term in the equations of motion. As expected,  $\int d\theta \rho_{ex}(\theta)$  grows exponentially. *Bottom:* In order to test convergence, the difference between the magnitude of  $\int d\theta \rho_{ex}(\theta)$  computed with 150 and 300 angular bins is shown as a function of time. All other input parameters are kept unchanged. Numerical convergence within  $\mathcal{O}(1\%)$  error is achieved in the non-linear regime.

severe by employing higher order derivatives instead of the usual central point method. In our code, we use a 7 point stencil which is accurate up to sixth order for spatial derivatives [34]. For the temporal evolution we use the Runge-Kutta-Fehlberg(7,8) method from the odeint library of Boost [35].

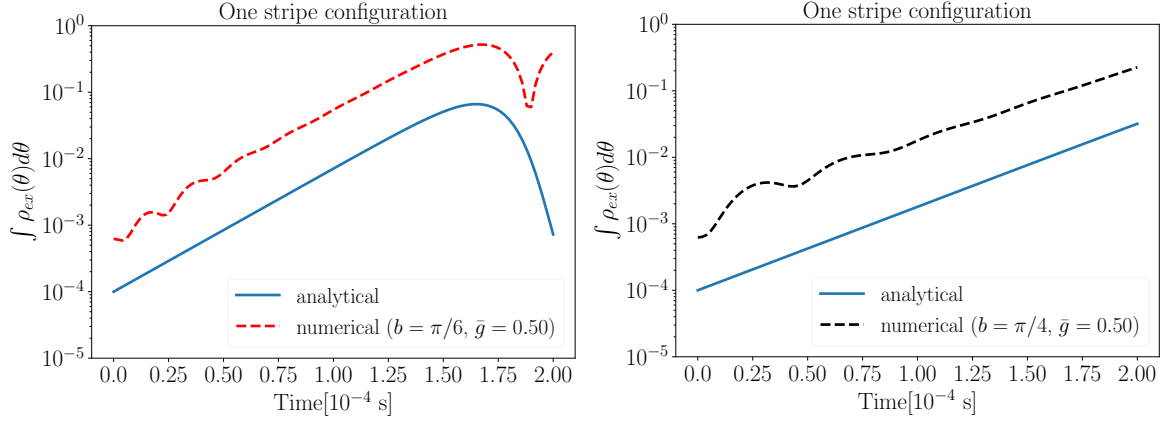
In order to speed up the computational time, we parallelize our numerical code through the OpenMP interface [36]. Within this simplified setup, each simulation run takes about 200 CPU-hours.

Figure 2 shows an example of the outcome of our simulation for the “one stripe configuration” (top middle of Fig. 1), with  $b = \pi/6$  and  $\bar{g} = 0.5$ . Moreover, we assume the following for the off-diagonal seeds:  $\rho_{ex}(\theta, t = 0 \text{ s}) = 10^{-4} \cos(2\pi y/L_y)$ , with  $y \in [0, L_y]$  such that the symmetry along the  $y$  direction is broken, and  $\bar{\rho}_{ex}(\theta, t = 0 \text{ s}) = 3\rho_{ex}(\theta, t = 0 \text{ s})$ <sup>1</sup>. In order to test convergence in the angular binning, we have ignored the advective term in the equations of motion for this run and will investigate its impact in Sec. 4. The top panel of Fig. 2 shows the off-diagonal term of the density matrix  $\int d\theta \rho_{ex}(\theta)$  as a function of time for a comoving point with maximum  $\rho_{\text{tot}} = \rho_{ee} + \bar{\rho}_{ee} + 2\rho_{xx} = \text{const.}$  in the box. As we will discuss in Sec. 3.3,  $\int d\theta \rho_{ex}(\theta)$  grows exponentially. When the magnitude of the off-diagonal elements of the density matrix reaches the same order as the diagonal elements ( $\sim \rho_{ee}$ ), flavor transformations start. Note that, in order to keep the computational time limited and since we focus on a simplified scenario, we only evolve the simulations for  $\mathcal{O}(10^{-4} \text{ s})$ , which corresponds to the time scale of interest in SNe or compact binary mergers.

The bottom panel of Fig. 2 is a convergence test of our results and it shows the error

<sup>1</sup>The off-diagonal seeds are such that  $\int d\theta [\rho_{ex}(\theta)/(\rho_{ee}(\theta) + \rho_{xx}(\theta))] = \int d\theta [\bar{\rho}_{ex}(\theta)/(\bar{\rho}_{ee}(\theta) + \bar{\rho}_{xx}(\theta))]$ .





**Figure 3.** Growth rate of  $\int d\theta \rho_{ex}(\theta)$  as a function of time for one comoving point in the box (“one stripe configuration”) from numerical simulations (dashed lines) compared with the analytical approximation of Eq. 3.5 (continuous lines) for two different opening widths of the  $\nu_e$  angular distribution ( $b = \pi/6$  for the panel on the left and  $b = \pi/4$  for the panel on the right) and isotropic  $\bar{\nu}_e$  distribution. The analytical expression of Eq. 3.5 perfectly matches the numerical growth rate of the instability.

in  $\int d\theta \rho_{ex}(\theta)$  for 150 and 300 uniformly distributed angle bins. We find that the results are identical within 1%.

### 3.3 Growth of the flavor instability

As shown in Fig. 2, when the advective term is neglected in Eqs. 2.2 and 2.3, the absolute value of the off-diagonal component of  $\rho$  grows exponentially in time. We find that the exponent,  $\kappa$ , satisfies the following proportionality

$$\kappa \propto \mu_{\text{eff}} \zeta \quad (3.5)$$

with

$$\mu_{\text{eff}} = \mu \int_0^{2\pi} d\theta [(\rho_{ee}(\theta) - \rho_{xx}(\theta)) - (\bar{\rho}_{ee}(\theta) - \bar{\rho}_{xx}(\theta))] , \quad (3.6)$$

where this definition of  $\mu_{\text{eff}}$  depends on the ELN, while the one of  $\mu$  in Eq. 2.5 is meant to be related to the total (anti)neutrino number density.

The growth of the flavor instability is shown in Fig. 3 where  $\int d\theta \rho_{ex}(\theta)$  is plotted as dashed line as a function of time for  $b = \pi/6$  (on the left) and  $b = \pi/4$  (on the right),  $\bar{g} = 0.5$ ,  $\rho_{ex}(\theta, t = 0 \text{ s}) = 10^{-4} \cos(2\pi y/L_y)$ , and  $\bar{\rho}_{ex}(\theta, t = 0 \text{ s}) = 3\rho_{ex}(\theta, t = 0 \text{ s})$  for the “one stripe configuration” and for one comoving point in the box. The continuous lines have been obtained by using Eq. 3.5. As one can see, Eq. 3.5 perfectly catches the growth rate of the off-diagonal terms of the density matrix. It should be noted that the definition of  $\kappa$  is heuristic in nature; although it is not clear whether a single parameter can encapsulate the growth rate of the instability for all angular distributions, the parametrization in Eq. 3.5 works for all cases that we have explored. When  $\vec{v} \cdot \nabla = 0$ , the exponential growth of the off-diagonal term of  $\rho$  does not depend on the neighboring regions, and it continues to grow until the non-linear regime is reached.

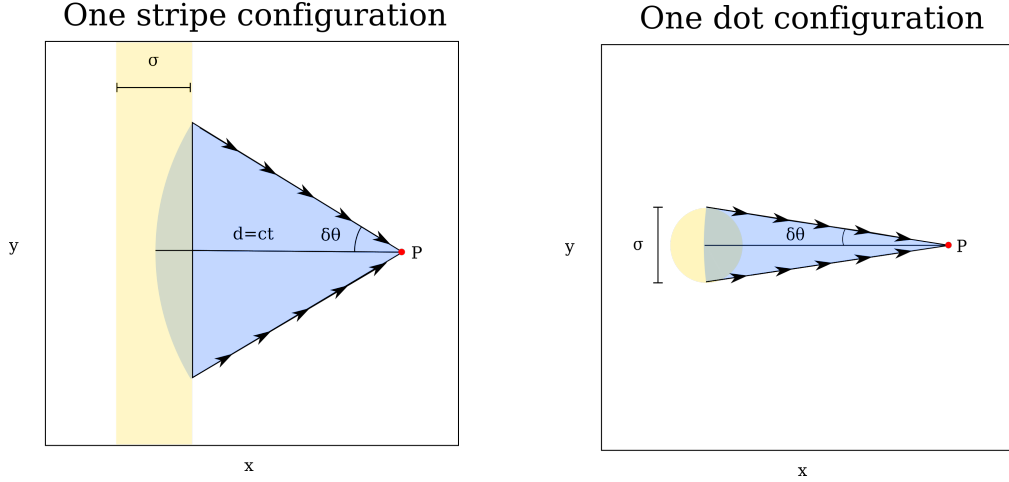


**Figure 4.** *Left:* Schematic diagram of the box in the “one stripe configuration.” Within the yellow stripe, ELN crossings are distributed in the plane following a Gaussian distribution of width  $\sigma$ . After a time  $t$ , the neutrino angular distribution in  $P$  will have maximum opening angle  $\delta\theta$  because of geometric effects. *Right:* Schematic diagram of the box in the “one dot configuration.” Unlike the stripe configuration, the maximum width of the angular distribution  $\delta\theta$  is determined by the dot size in the dot configuration.

## 4 Role of the advective term in the neutrino evolution equation

In this Section, after general considerations on the impact of the advective term, we discuss the role that the latter plays on the growth of flavor instabilities in the “one stripe configuration,” “two stripe configuration,” and in the “one dot configuration.” We also discuss how advection affects the evolution of the ELN distribution as a function of time. In this Section, we assume  $\rho_{ex}(\theta, t = 0 \text{ s}) = 10^{-3} \cos(2\pi y/L_y)$  and  $\bar{\rho}_{ex}(\theta, t = 0 \text{ s}) = 3\rho_{ex}(\theta, t = 0 \text{ s})$  in all numerical runs.

### 4.1 Impact of the advective term on the neutrino distributions

Before exploring the growth of the flavor instabilities in the different configurations assumed for our 2D box, we adopt geometrical arguments to forecast how the angular distributions should evolve in the presence of advection.

The left panel of Fig. 4 shows a schematic diagram of the box in the “one stripe configuration.” Let us consider a point  $P = (x, y)$  outside the initial location of the stripe ( $|(x - x_0)| > \sigma$ ). At  $t \sim (x - x_0)/c$ , neutrinos from various points along the stripe and emitted along different  $\theta$ ’s will reach  $P$ .

It is easy to estimate the width of the angular distribution at any given time, which is dependent on the width of the initial distribution  $b(\bar{b})$ , see Eqs. 3.1-3.3. If the width of the initial distribution is zero (i.e., we start with Dirac delta function), then at any given time  $t$ , only neutrinos traveling along a certain direction can reach the point  $P$ . In other words, for any point  $P$  that was not on the stripe initially, the angular distribution will still be a Dirac delta distribution in  $\theta$ .

Understanding the limiting case with  $b(\bar{b}) \rightarrow 0$  allows to draw insightful conclusions regarding the evolution of the ELN crossings in time. At any given point  $P$  far away from the stripe, there will be a wavefront of neutrinos that will pass through it at time  $t$  and if

the distance of  $P$  from  $x_0$  is greater than  $\sigma$  the argument from the previous paragraph will still hold. If the distance between  $P$  and  $x_0$  is  $d$ , then the width of the angular distribution at a certain time  $t$  will be

$$\delta\theta \approx \min \left[ w, \arctan \left( \sqrt{\frac{\sigma}{d}} \right) \right], \quad (4.1)$$

where  $w$  is the width of the initial angular distribution, which is  $b$  or  $\bar{b}$  (Eqs. 3.2 and 3.3). Equation 4.1 is such that no matter how large  $\sigma$  is, the angular width cannot be greater than  $w$ . The second argument of the min function in Eq. 4.1 can be easily gleaned by noticing that the width of the angular distribution is given by the neutrino which is emitted at  $x - x_0 = \sigma$ . If  $\arctan \left( \sqrt{\sigma/d} \right) < w$ , then the angular distributions of  $\nu_e$  and  $\bar{\nu}_e$  have the same width, and fast conversions cannot occur.

In the “two stripe configuration,” if we focus on the limit  $b(\bar{b}) \rightarrow 0$  then, in order to reach a point  $P$  outside both stripes at time  $t$ , neutrinos will have traveled different path-lengths; hence, their angular distributions will be peaked at different  $\theta$ 's. As a consequence, the instability parameter  $\zeta$  which was initially zero for all points in between the two stripes will become non-zero. As we will discuss in Sec. 4.3, this means that this configuration may probably favor the growth of flavor instabilities.

Similar considerations hold for the “one dot configuration,” see the right panel of Fig. 4. Let us consider a point  $P = (x, y)$  outside the “dot” in the 2D box, i.e.  $d^2 = (x - x_0)^2 + (y - y_0)^2 > \sigma^2$ . From simple geometric considerations, it can be seen that the advective term acts like a narrow pass filter. In fact, at  $t$  the (anti)neutrino angular distribution will have width

$$\delta\theta \approx \min \left[ w, \arctan \left( \frac{\sigma}{d} \right) \right], \quad (4.2)$$

where  $w$  is the width of the initial angular distribution of neutrinos or antineutrinos. Notably, the rate at which the neutrino number density dilutes as a result of advection is different for the “one stripe” and for the “dot” configurations.

We now explore the role of the advective term in the neutrino equations of motion. We expect that the advective term will have several effects on the neutrino flavor evolution. On the one hand, the advective term should diffuse any eventual ELN excess localized in a small spatial region, diluting it over a broader region. On the other hand, the parameter  $\zeta$  should be modified as a result of advection. Moreover, as it will become clear in the following, by modifying the instability parameter, the advective term will also affect the occurrence of fast conversions.

The time-scale required for the advective term to wipe out the instability parameter ( $\zeta \rightarrow 0$ ) is given by the time at which the two arguments of the min function in Eq. 4.1 are comparable:

$$t_{\text{conv}} \approx \frac{\sigma}{w^2}. \quad (4.3)$$

In this case, the width of the angular distribution of  $\nu_e$  and  $\bar{\nu}_e$  becomes independent of the initial angular distribution, and it is the same for  $\nu_e$  and  $\bar{\nu}_e$ .

The characteristic time scale of neutrino advection,  $t_{\text{conv}}$ , should be compared with the other characteristic time scale of the system  $t_{\text{osc}}$ , which defines the time required for flavor transformations to occur. In fact, because of flavor instabilities, the off-diagonal term of the density matrix evolves like  $\rho_{ex}(t = 0) \exp(\kappa t_{\text{osc}}) = \mathcal{O}(\rho_{ee})$ ;  $t_{\text{osc}}$  obviously depends on the initial magnitude of the off-diagonal term, the effective neutrino number density, and  $\zeta$ . In turn, the latter two evolve in time because of the advective term in the equations of motion.

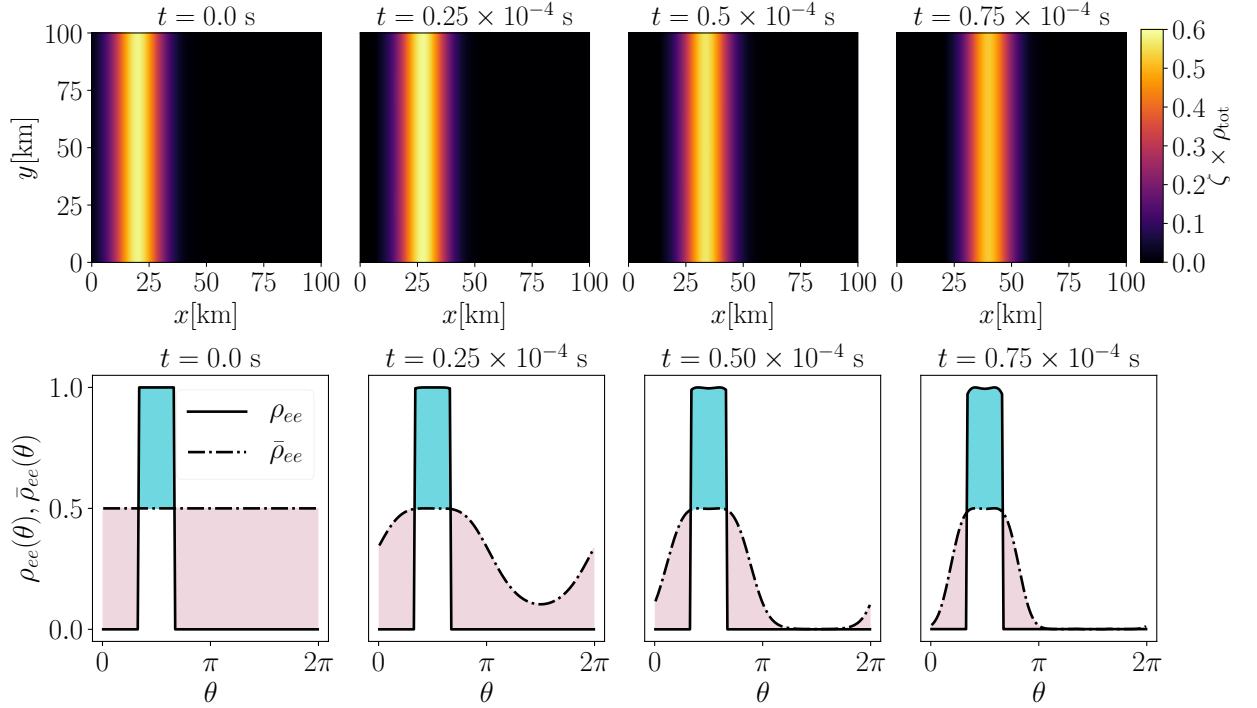


**Figure 5.** *Top:* Evolution of  $\zeta \times \rho_{\text{tot}}$  in the 2D box for the “one stripe configuration” (see Eq. 2.6 and Fig. 1). The time snapshots for the four panels are  $t = 0.0, 0.25 \times 10^{-4}, 0.5 \times 10^{-4}$  and  $0.75 \times 10^{-4}$  s from left to right, respectively. *Bottom:* Angular distributions of  $\nu_e$  (continuous line) and  $\bar{\nu}_e$  (dashed line) as a function of  $\theta$  for a comoving point in the box with the maximum  $\rho_{\text{tot}}(x, y)$ . The instability parameter  $\zeta \neq 0$  (see Eq. 2.6) when both the cyan and magenta areas are non-zero and it is proportional to the product of the two areas. While  $\rho_{\text{tot}} = \text{const.}$ , the effect of neutrino propagation is to reduce  $\zeta$  by spreading the angular distributions as a function of  $\theta$  as  $t$  increases.

## 4.2 Flavor evolution in the one stripe configuration

We will now focus on the “one stripe configuration” of our 2D box, see the left top panel of Fig. 1. We investigate the flavor evolution in the presence of the advective term in the neutrino equations of motion, assuming  $b = \pi/6$  and  $\bar{g} = 0.5$  (see Sec. 3.1 for more details).

The top panels of Fig. 5 show the resultant evolution of  $\zeta \times \rho_{\text{tot}}$  with  $\zeta$  defined as in Eq. 2.6 and  $\rho_{\text{tot}} = \rho_{ee} + \bar{\rho}_{ee} + 2\rho_{xx} = \text{const.}$  for  $t = 0.0, 0.25 \times 10^{-4}, 0.5 \times 10^{-4}$  and  $0.75 \times 10^{-4}$  s, from left to right respectively. Because of advection, the initial stripe tends to drift from left to right in the box as time increases. The corresponding bottom panels show the  $\nu_e$  and  $\bar{\nu}_e$  angular distributions of the comoving point with maximum  $\rho_{\text{tot}}(x, y)$  for each time snapshot. The  $\nu_e$  and  $\bar{\nu}_e$  angular distributions evolve such that  $\zeta$  is large at  $t = 0$  s, but  $\zeta$  starts decreasing as time increases since the neutrino distributions become more and more forward peaked. Although we show the angular distributions for a selected comoving point, this trend holds for all points in the 2D box. Animations of  $\zeta \times \rho_{\text{tot}}$ ,  $\nu_e$  and  $\bar{\nu}_e$  angular distributions, and of the diagonal and off-diagonal terms of the neutrino and antineutrino density matrix are provided as [Supplemental Material](#).

We investigate whether advection hinders the development of fast neutrino oscillations within the “stripe ELN configuration.” The left panel of Fig. 6 shows the evolution of  $\hat{\rho}_{ex} = (\int |\rho_{ex}| dx dy d\theta) / [\int (\rho_{ee} + \rho_{xx}) dx dy d\theta]$  and  $\hat{\bar{\rho}}_{ex}$  (defined analogously to  $\hat{\rho}_{ex}$ ) as a function

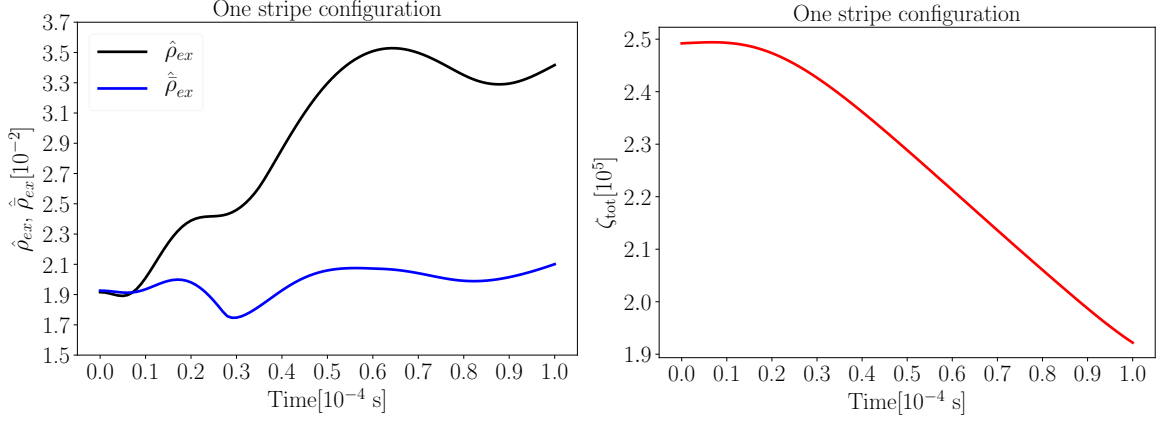


**Figure 6.** *Left:* Evolution of  $\hat{\rho}_{ex} = (\int |\rho_{ex}| dx dy d\theta) / [\int (\rho_{ee} + \rho_{xx}) dx dy d\theta]$  and  $\hat{\bar{\rho}}_{ex}$  as a function of time. *Right:* Temporal evolution of the total instability parameter ( $\zeta_{tot} = \int dx dy \zeta$ ). As a consequence of advection,  $\hat{\rho}_{ex}$  and  $\hat{\bar{\rho}}_{ex}$  reach a plateau at about  $0.6 \times 10^{-4}$  s and the integrated instability parameter decreases with time.

of time. In the absence of convection, the off-diagonal terms grow exponentially (see left panel of Fig. 3), but now  $\hat{\rho}_{ex}$  and  $\hat{\bar{\rho}}_{ex}$  reach a plateau at  $t \simeq 0.6 \times 10^{-4}$  s. In fact, as a consequence of the role played by the advective term,  $\zeta_{tot} = \int \zeta dx dy$  decreases with time as the neutrino and antineutrino angular distributions tend to be more and more forward peaked, see right panel of Fig. 6 and bottom panel of Fig. 5.

This configuration of the 2D box tends to mimic what would happen in a SN patch in the presence of a front of ELN crossings. As one can see, unless the ELN crossings are self-sustained (as it could be in the case of LESA), they would be wiped out by the neutrino advective term. As a consequence, fast pairwise conversions would only lead to partial flavor conversion. Notably, our setup overestimates the effect of flavor conversions since we assume  $\mu = \text{const.}$  in the box and maximize the initial  $\zeta$  by assuming an isotropic distribution for  $\bar{\nu}_e$ . In a realistic case,  $\mu$  would tend to decrease as the distance from the decoupling region increases and  $\zeta(t = 0 \text{ s})$  would be likely smaller than in our case given that the angular distribution of  $\bar{\nu}_e$  is not isotropic outside the proto-neutron star radius.

### 4.3 Flavor evolution in the two stripe configuration

We now explore the “two stripe configuration” of our 2D box, see middle top panel of Fig. 1. As we will see, in this configuration, the advective term in the neutrino equation of motion may create conditions that are favorable for fast pairwise conversions.

We evolve the (anti)neutrino field in time for two identical stripes moving in opposite directions ( $b = \pi/6$  and  $\bar{g} = 0.5$ , see Sec. 3.1 for more details). Animations of  $\zeta \times \rho_{tot}$ ,  $\nu_e$  and  $\bar{\nu}_e$  angular distributions, the diagonal and off-diagonal terms of the neutrino and antineutrino density matrices are provided as [Supplemental Material](#).

As shown in Fig. 7, the two stripes move towards each other until they cross and then keep moving in opposite directions. The angular distributions of  $\nu_e$  and  $\bar{\nu}_e$  are initially identical in the two stripes. As the stripes evolve towards each other, for a comoving point  $(x, y)$  in the 2D box, the angular distributions of  $\nu_e$  and  $\bar{\nu}_e$  start to develop two peaks (one along  $\theta = \pi/2$  and one along  $\theta = 3\pi/2$ ), corresponding to the forward and backward directions with respect to  $\vec{v}$ . The encounter of the two stripes at  $t \simeq 0.5 \times 10^{-4}$  s leads

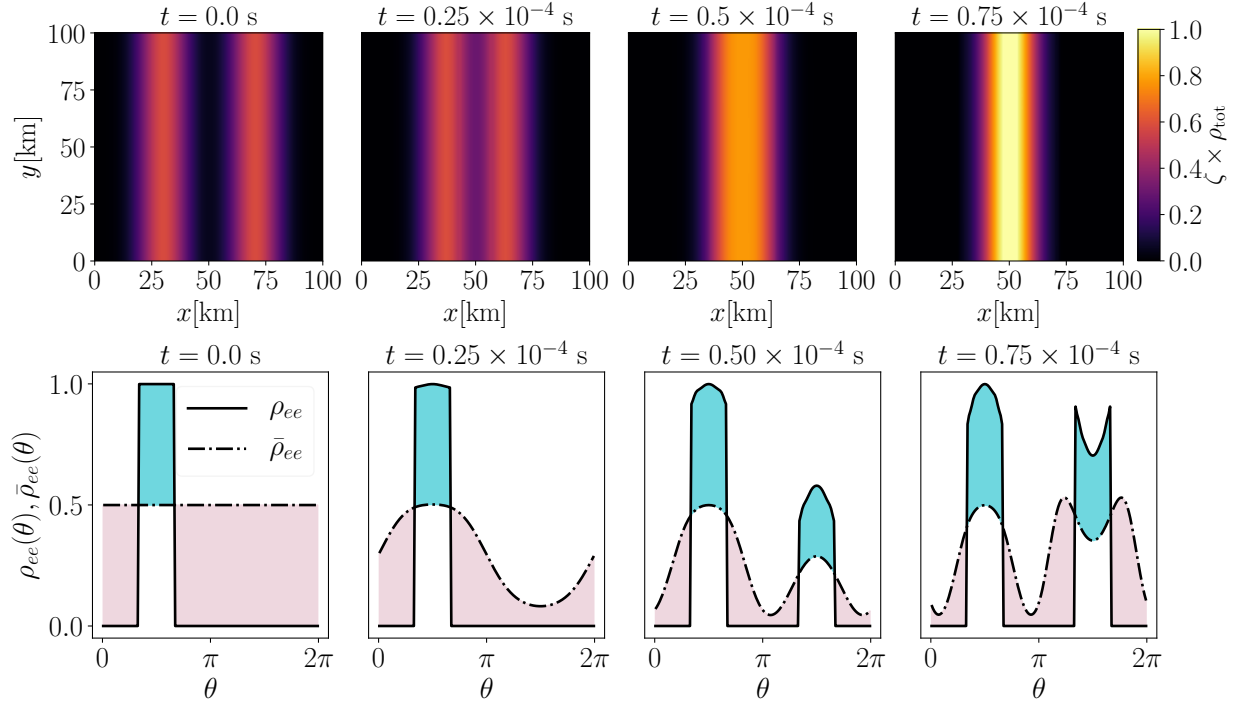


**Figure 7.** Same as Fig. 5 but for the “two stripe configuration.” Note that the  $\nu_e$  angular distribution shown in the bottom panels has one peak at  $t = 0$  s, but it develops two peaks as  $t$  increases when it encounters neutrinos traveling in the opposite direction from the other stripe.

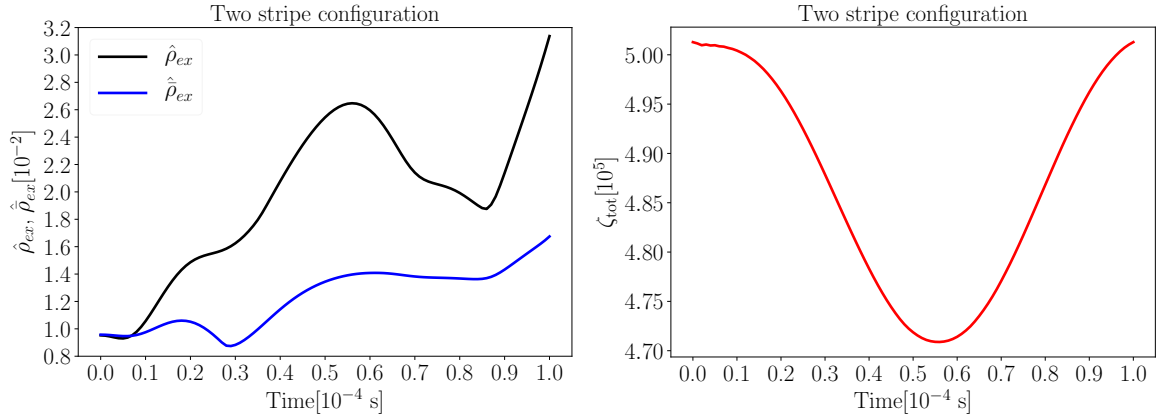


**Figure 8.** Same as Fig. 6 but for the “two stripe configuration.” As a consequence of advection, the off-diagonal terms  $\hat{\rho}_{ex}$  and  $\hat{\bar{\rho}}_{ex}$ , reach a plateau as the instability parameter  $\zeta_{\text{tot}}$  decreases until  $t \simeq 0.5 \times 10^{-4}$  s. The latter gradually increases for  $t \geq 0.5 \times 10^{-4}$  s as the neutrinos from one stripe encounter neutrinos from the stripe; correspondingly the off-diagonal terms  $\hat{\rho}_{ex}$  and  $\hat{\bar{\rho}}_{ex}$  tend to increase again.

to a buildup of  $\zeta \times \rho_{\text{tot}}$ ; this dynamically generates favorable conditions for fast pairwise conversions.

Figure 8 shows the evolution of  $\hat{\rho}_{ex}$  and  $\hat{\bar{\rho}}_{ex}$  (on the left) and  $\zeta_{\text{tot}}$  (on the right) as a function of time. Similarly to what discussed in Sec. 4.2, the advective term tends to erase

the conditions required for fast pairwise conversions before the two stripes meet. However, as the two stripes cross each other at  $t \simeq 0.5 \times 10^{-4}$  s,  $\zeta_{\text{tot}}$  starts to grow again. The off-diagonal terms of the density matrices ( $\hat{\rho}_{ex}$  and  $\hat{\bar{\rho}}_{ex}$ ) tend to increase, correspondingly. Note, however, that such a dynamical generation of favorable conditions for fast pairwise conversions ends as soon as the two stripes pass each other, as also shown in the [movies](#).

A situation similar to the one discussed here may happen in compact binary mergers or in SNe when a non-negligible backward flux (with respect to the  $\vec{v}$  direction) of neutrinos is present, see e.g. Refs. [23, 28]. In fact, in this case, a spatial instability would develop leading to fast pairwise conversions [16]. Notably, what is described as backward flux in Ref. [28] is dependent on the reference frame of the observer; any angular distributions of  $\nu_e$  and  $\bar{\nu}_e$  such that there is a significant backward flux of one with respect to the other in any reference frame will lead to fast neutrino conversions.

Importantly, such configuration would lead to sustained flavor conversions only in the presence of a stationary flux of (anti)neutrinos moving backward and forward with respect to  $\vec{v}$ . This could only happen in the proximity of the neutrino decoupling region. Note, however, that collisions would also matter in the proximity of the decoupling region. Although they have been neglected in this work, it could be that they will contribute to damp the instability, preventing its growth.

#### 4.4 Flavor evolution in the one dot configuration

We also consider another class of initial conditions: when neutrinos and antineutrinos are initially localized within a dot in the  $(x, y)$  box (“one dot configuration”), see Eq. 3.4 and the right top panel of Fig. 1. The general principle governing the relationship between convection and flavor evolution remains similar to the one discussed for the stripe configuration, but quantitatively different. In fact, as we will see, the advective term acts like a narrow pass filter for certain angular modes, while at the same time diluting the number density of neutrinos.

We assume the initial angular distributions as described in Sec. 3.1 and fix  $b = \pi/6$  and  $\bar{g} = 0.5$ . We provide animations of  $\zeta \times \rho_{\text{tot}}$ ,  $\nu_e$  and  $\bar{\nu}_e$  angular distributions, the diagonal and off-diagonal terms of the neutrino and antineutrino density matrices as [Supplemental Material](#).

In Fig. 9, we show the evolution of neutrino  $\zeta \times \rho_{\text{tot}}$  for the one dot configuration of the 2D box and the corresponding evolution of the angular distributions. Unlike the “stripe configuration,” the number density falls very rapidly (cfr. Fig. 5), as also discussed in Sec. 4.1.

The left panel of Fig. 10 shows the evolution of the off-diagonal terms of the density matrices,  $\hat{\rho}_{ex}$  and  $\hat{\bar{\rho}}_{ex}$ , as a function of time. The panel on the right shows the evolution of the instability parameter  $\zeta_{\text{tot}}$ . In this case,  $\hat{\rho}_{ex}$  and  $\hat{\bar{\rho}}_{ex}$  decrease for  $t \geq 0.2 \times 10^{-4}$  s as the instability parameter  $\zeta_{\text{tot}}$  decreases. This is a direct consequence of the rapid diffusion of the ELN excess.

This configuration mimics what would happen in SNe or compact binary mergers in the presence of localized ELN excess, e.g. generated by stochastic hydrodynamical fluctuations. We can conclude that this configuration would not lead to major changes in the flavor configuration and would be negligible for what concerns fast pairwise conversions.

## 5 Outlook and conclusions

Compact astrophysical objects are so dense in neutrinos that quantum effects are expected to manifest at macroscopic scales. In this work, we explore an interesting and insightful

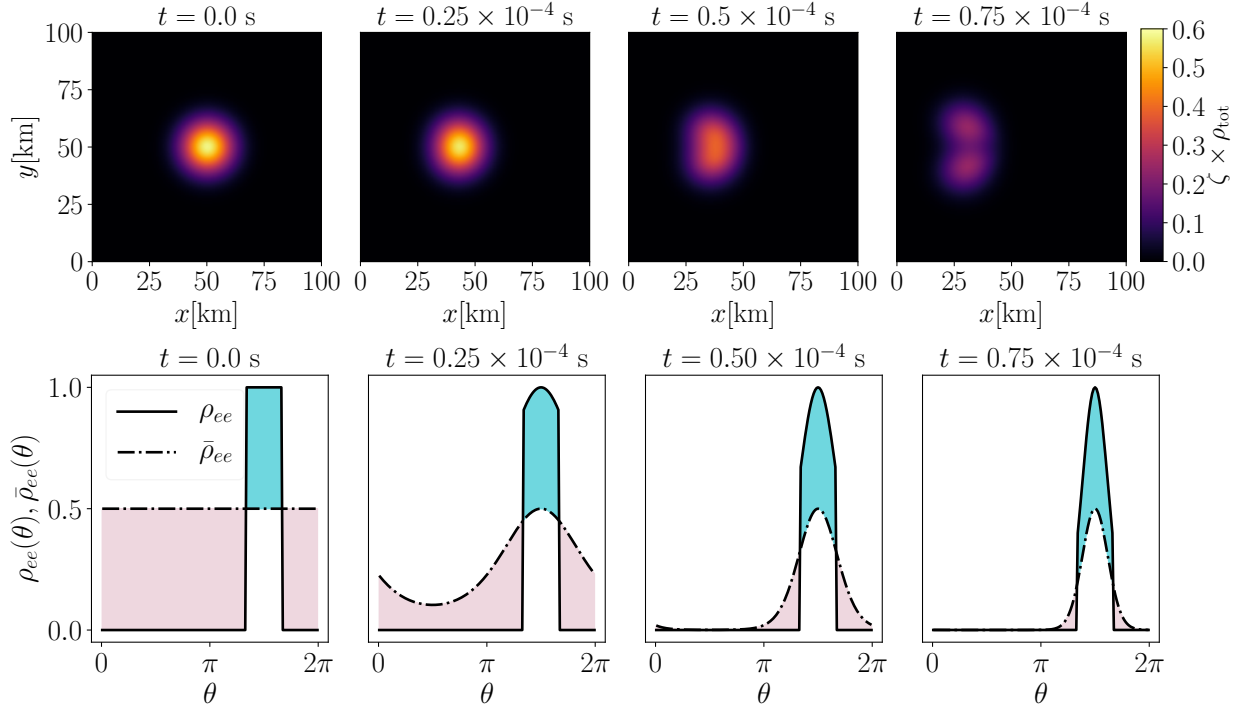


**Figure 9.** Same as Fig. 5, but for the “one dot configuration” of the 2D box. The  $\zeta \times \rho_{\text{tot}}$  parameter, which is proportional to the product of the areas of the cyan and magenta regions, decreases faster compared to Fig. 5.

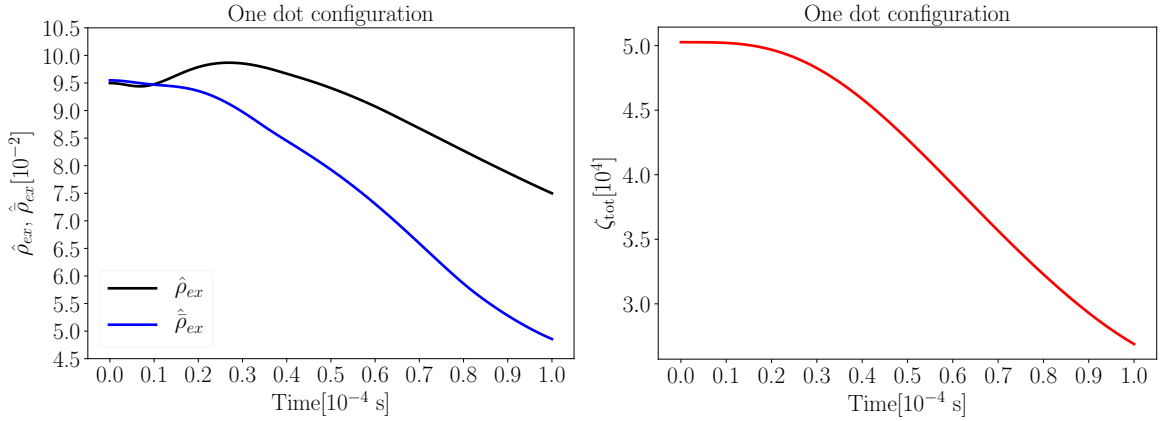


**Figure 10.** Same as Fig. 6 but for the “one dot configuration.” As a consequence of advection, the off-diagonal terms of the density matrices ( $\hat{\rho}_{ex}$  and  $\hat{\bar{\rho}}_{ex}$ ) starts to decrease at  $t \simeq 0.2 \times 10^{-4}$  s as the instability parameter  $\zeta_{\text{tot}}$  decreases.

interplay between the neutrino pairwise conversions (quantum effect) and the propagation of the neutrino field driven by the advective term in the equations of motion (classical effect). In order to do this, for the first time, we track the neutrino flavor evolution within a (2+1+1) framework, i.e. we solve the neutrino equations of motion in time, two spatial dimensions, and one angular variable.



We explore a simplified scenario with constant neutrino–neutrino potential for the sake of simplicity, however we mimic configurations similar to the ones that could occur in compact astrophysical objects where favorable conditions for fast pairwise conversions have been found through the stability analysis. In particular, we explore three different configurations: 1. neutrinos and antineutrinos are initially localized along one stripe in our 2D box, mimicking a situation similar to LESA; 2. two fronts of neutrinos and antineutrinos moving towards each other, similar to what could happen in the proximity of the neutrino decoupling region; 3. one localized excess of particles with electron lepton number (ELN) crossings, mimicking ELN fluctuations that could occur because of stochastic hydrodynamical fluctuations.

We generalize the conditions leading to the development of fast pairwise conversions introducing the instability parameter  $\zeta$  that broadly captures the essence of the shape of the neutrino angular distributions leading to flavor instabilities. The instability parameter  $\zeta$  along with the effective strength of neutrino-neutrino interactions determines the instantaneous growth rate of the off-diagonal components of the density matrices. However, the numerical solution of the neutrino equations of motion highlights a fascinating interplay between the growth of fast pairwise conversions and neutrino advection. Our sophisticated numerical simulations show that the advective term in the equations of motion hinders the growth of flavor instabilities, unless the front of ELN crossings (or of neutrinos moving in the opposite direction of  $\vec{v}$ ) is self-sustained in time.

As a consequence, our simple model predicts that significant flavor evolution due to fast pairwise conversions can occur in the presence of the LESA instability (scenario 1), but would not be significant for a localized ELN excess (scenario 3). Interestingly, in the proximity of the decoupling region where neutrinos are streaming backward and forward with respect to the emission direction, the angular distributions can evolve dynamically because of the advective term leading to the dynamical development of favorable conditions for fast pairwise conversions (scenario 2); a more in-depth analysis including collisions is however mandatory in this latter case, since collisions may damp the growth of flavor instabilities.

This work demonstrates a critical limitation of the linear stability analysis widely used in the field of collective neutrino conversions, as the time scales that are relevant from the point of view of classical evolution (i.e., advection) may be comparable to the time scale of flavor conversions. In addition, the advective term in the equations of motion is such that the conditions leading to the growth of flavor instabilities are dynamically affected from the surroundings. This aspect is not captured by the stability analysis.

Ours is the first numerical solution of the neutrino flavor evolution within a sophisticated and dynamical multi-dimensional framework. Although our work is in no way the final setup resembling the evolution of the neutrino field in core-collapse supernovae or compact binary mergers, it highlights the dynamical nature of flavor evolution.

## Acknowledgments

We are grateful to the Villum Foundation (Project No. 13164), the Danmarks Frie Forskningsfonds (Project No. 8049-00038B), the Knud Højgaard Foundation, and the Deutsche Forschungsgemeinschaft through Sonderforschungsbereich SFB 1258 “Neutrinos and Dark Matter in Astro- and Particle Physics” (NDM).

## References

- [1] L. Wolfenstein, *Neutrino Oscillations in Matter*, *Phys. Rev.* **D17** (1978) 2369–2374.
- [2] S. P. Mikheyev and A. Yu. Smirnov, *Resonance Amplification of Oscillations in Matter and Spectroscopy of Solar Neutrinos*, *Sov. J. Nucl. Phys.* **42** (1985) 913–917.
- [3] A. Mirizzi, I. Tamborra, H.-T. Janka, N. Saviano, K. Scholberg, R. Bollig et al., *Supernova Neutrinos: Production, Oscillations and Detection*, *Riv. Nuovo Cim.* **39** (2016) 1–112, [[1508.00785](#)].
- [4] H. Duan, G. M. Fuller and Y.-Z. Qian, *Collective Neutrino Oscillations*, *Ann. Rev. Nucl. Part. Sci.* **60** (2010) 569–594, [[1001.2799](#)].
- [5] H. Duan, G. M. Fuller and Y.-Z. Qian, *Collective neutrino flavor transformation in supernovae*, *Phys. Rev.* **D74** (2006) 123004, [[astro-ph/0511275](#)].
- [6] H. Duan, G. M. Fuller, J. Carlson and Y.-Z. Qian, *Simulation of Coherent Non-Linear Neutrino Flavor Transformation in the Supernova Environment. 1. Correlated Neutrino Trajectories*, *Phys. Rev.* **D74** (2006) 105014, [[astro-ph/0606616](#)].
- [7] H. Duan, G. M. Fuller, J. Carlson and Y.-Z. Qian, *Coherent Development of Neutrino Flavor in the Supernova Environment*, *Phys. Rev. Lett.* **97** (2006) 241101, [[astro-ph/0608050](#)].
- [8] G. L. Fogli, E. Lisi, A. Marrone and A. Mirizzi, *Collective neutrino flavor transitions in supernovae and the role of trajectory averaging*, *JCAP* **0712** (2007) 010, [[0707.1998](#)].
- [9] G. L. Fogli, E. Lisi, A. Marrone, A. Mirizzi and I. Tamborra, *Low-energy spectral features of supernova (anti)neutrinos in inverted hierarchy*, *Phys. Rev.* **D78** (2008) 097301, [[0808.0807](#)].
- [10] A. Banerjee, A. Dighe and G. G. Raffelt, *Linearized flavor-stability analysis of dense neutrino streams*, *Phys. Rev.* **D84** (2011) 053013, [[1107.2308](#)].
- [11] G. G. Raffelt, S. Sarikas and D. de Sousa Seixas, *Axial Symmetry Breaking in Self-Induced Flavor Conversion of Supernova Neutrino Fluxes*, *Phys. Rev. Lett.* **111** (2013) 091101, [[1305.7140](#)].
- [12] H. Duan and S. Shalgar, *Flavor instabilities in the neutrino line model*, *Phys. Lett.* **B747** (2015) 139–143, [[1412.7097](#)].
- [13] S. Abbar, H. Duan and S. Shalgar, *Flavor instabilities in the multiangle neutrino line model*, *Phys. Rev.* **D92** (2015) 065019, [[1507.08992](#)].
- [14] R. F. Sawyer, *The multi-angle instability in dense neutrino systems*, *Phys. Rev.* **D79** (2009) 105003, [[0803.4319](#)].
- [15] R. F. Sawyer, *Neutrino cloud instabilities just above the neutrino sphere of a supernova*, *Phys. Rev. Lett.* **116** (2016) 081101, [[1509.03323](#)].
- [16] I. Izaguirre, G. G. Raffelt and I. Tamborra, *Fast Pairwise Conversion of Supernova Neutrinos: A Dispersion-Relation Approach*, *Phys. Rev. Lett.* **118** (2017) 021101, [[1610.01612](#)].
- [17] F. Capozzi, B. Dasgupta, A. Mirizzi, M. Sen and G. Sigl, *Collisional triggering of fast flavor conversions of supernova neutrinos*, *Phys. Rev. Lett.* **122** (2019) 091101, [[1808.06618](#)].
- [18] B. Dasgupta, A. Mirizzi and M. Sen, *Fast neutrino flavor conversions near the supernova core with realistic flavor-dependent angular distributions*, *JCAP* **1702** (2017) 019, [[1609.00528](#)].
- [19] F. Capozzi, B. Dasgupta, E. Lisi, A. Marrone and A. Mirizzi, *Fast flavor conversions of supernova neutrinos: Classifying instabilities via dispersion relations*, *Phys. Rev.* **D96** (2017) 043016, [[1706.03360](#)].
- [20] C. Yi, L. Ma, J. D. Martin and H. Duan, *Dispersion relation of the fast neutrino oscillation wave*, *Phys. Rev.* **D99** (2019) 063005, [[1901.01546](#)].

- [21] S. Shalgar and I. Tamborra, *On the Occurrence of Crossings Between the Angular Distributions of Electron Neutrinos and Antineutrinos in the Supernova Core*, *Astrophys. J.* **883** (2019) 80, [[1904.07236](#)].
- [22] T. Morinaga, H. Nagakura, C. Kato and S. Yamada, *A new possibility of the fast neutrino-flavor conversion in the pre-shock region of core-collapse supernova*, [1909.13131](#).
- [23] M.-R. Wu and I. Tamborra, *Fast neutrino conversions: Ubiquitous in compact binary merger remnants*, *Phys. Rev.* **D95** (2017) 103007, [[1701.06580](#)].
- [24] M.-R. Wu, I. Tamborra, O. Just and H.-T. Janka, *Imprints of neutrino-pair flavor conversions on nucleosynthesis in ejecta from neutron-star merger remnants*, *Phys. Rev.* **D96** (2017) 123015, [[1711.00477](#)].
- [25] I. Tamborra, L. Hüpdepohl, G. G. Raffelt and H.-T. Janka, *Flavor-dependent neutrino angular distribution in core-collapse supernovae*, *Astrophys. J.* **839** (2017) 132, [[1702.00060](#)].
- [26] S. Abbar, H. Duan, K. Sumiyoshi, T. Takiwaki and M. C. Volpe, *Fast Neutrino Flavor Conversion Modes in Multidimensional Core-collapse Supernova Models: the Role of the Asymmetric Neutrino Distributions*, [1911.01983](#).
- [27] S. Abbar, H. Duan, K. Sumiyoshi, T. Takiwaki and M. C. Volpe, *On the occurrence of fast neutrino flavor conversions in multidimensional supernova models*, *Phys. Rev.* **D100** (2019) 043004, [[1812.06883](#)].
- [28] S. Abbar and H. Duan, *Fast neutrino flavor conversion: roles of dense matter and spectrum crossing*, *Phys. Rev.* **D98** (2018) 043014, [[1712.07013](#)].
- [29] M. Delfan Azari, S. Yamada, T. Morinaga, H. Nagakura, S. Furusawa, A. Harada et al., *Fast collective neutrino oscillations inside the neutrino sphere in core-collapse supernovae*, [1910.06176](#).
- [30] H. Nagakura, T. Morinaga, C. Kato and S. Yamada, *Fast-pairwise collective neutrino oscillations associated with asymmetric neutrino emissions in core-collapse supernova*, [1910.04288](#).
- [31] M. Delfan Azari, S. Yamada, T. Morinaga, W. Iwakami, H. Okawa, H. Nagakura et al., *Linear Analysis of Fast-Pairwise Collective Neutrino Oscillations in Core-Collapse Supernovae based on the Results of Boltzmann Simulations*, *Phys. Rev.* **D99** (2019) 103011, [[1902.07467](#)].
- [32] I. Tamborra, F. Hanke, H.-T. Janka, B. Müller, G. G. Raffelt and A. Marek, *Self-sustained asymmetry of lepton-number emission: A new phenomenon during the supernova shock-accretion phase in three dimensions*, *Astrophys. J.* **792** (2014) 96, [[1402.5418](#)].
- [33] J. D. Martin, C. Yi and H. Duan, *Dynamic fast flavor oscillation waves in dense neutrino gases*, *Phys. Lett.* **B800** (2020) 135088, [[1909.05225](#)].
- [34] Wikipedia, “Finite difference coefficient.” [https://en.wikipedia.org/wiki/Finite\\_difference\\_coefficient](https://en.wikipedia.org/wiki/Finite_difference_coefficient), 2019.
- [35] Boost, “Boost C++ Libraries.” <http://www.boost.org/>, 2019.
- [36] OpenMP.org, “The OpenMP API specification for parallel programming.” <http://openmp.org>, 2013.